ZnO Twin-Spheres Exposed in ±(001) Facets: Stepwise Self-Assembly Growth and Anisotropic Blue Emission

Feng Li,[*,†,‡,§] Feilong Gong,[†] Yuanhua Xiao,[†,§] Aiqin Zhang,[†,§] Jihong Zhao,[†] Shaoming Fang,[*,†] and Dianzeng Jia[§]

[†]State Laboratory of Surface and Interface Science and Technology, Zhengzhou University of Light Industry, Zhengzhou 450002, China, [‡]American Advanced Nanotechnology (AAN), Houston, Texas 77459, United States, and [§]Applied Chemical Institute, Xinjiang University, Urumqi, 830046, Xinjiang, China

ABSTRACT ZnO twin-spheres topologically exposed in ±(001) polar facets have been successfully produced on a large scale. The fragmentary and hexagonal ±(001) facets of ZnO tilt and assemble gradually for 8−12 generations to form supercrystals. The surfactant effect on the formation of ZnO supercrystals reveals that their structure stepwise evolves from prisms to dumbbells to twin-spheres exposed in ±(001) facets and eventually to twin-spheres covered with dots. A hollow ring around a prism, which connects two hemispheres of the supercrystals, is finally sealed inside each of the twin-spheres. Based on the experimental observations, a stepwise self-assembly mechanism is proposed to understand the formation of the supercrystals. It is also observed that the ZnO twin-spheres exhibit anisotropic blue emission in intensity attributed to their special surfaces exposed in ±(001) facets. Novel devices could be designed and fabricated through carefully tailoring the microstructure of ZnO supercrystals.

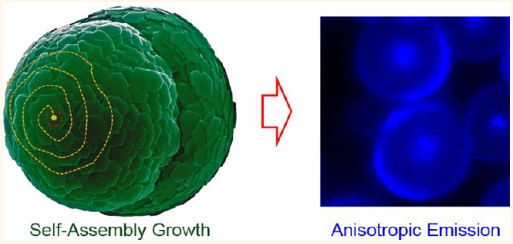

KEYWORDS: ZnO twin-spheres · supercrystals · ±(001) facets · self-assembly growth · anisotropic emission

Zinc oxide (ZnO) is an important material with diverse applications for its wurtzite crystal structure with a wide band gap of 3.37 eV.[1−33] The intrinsic high energy of the ±(001) polar surface of ZnO crystals leads to their fast growth along ⟨0001⟩, and therefore 1D hexagonal ZnO nanowires or nanorods exposed in (100) and (110) nonpolar facets are generally produced with different synthesis methods. ZnO nanocrystals exposed in ±(001) polar planes are therefore desired highly for the potential of further tailoring the functionalities of the materials and possibly enhancing their performance in applications such as sensors and catalysts. In contrast because the surface energy of crystals can be tuned by the external growth medium, single crystals exposed in special planes could be fabricated in wet chemical systems through carefully adjusting growth parameters such as temperature, solvents, and organic/inorganic additives. ZnO mesocrystals with stacked and layered superstructures exposed in ±(001) polar surfaces, for instance, can be produced by introducing organic additives into wet chemical reactions for inhibiting their growth rate along ⟨0001⟩. Based in this technique, Liu and his coworkers have made complex ZnO superstructures after adding sodium citrate into the hydrothermal growth system.[34−38] Helically stacked ZnO columns composed of thin layers exposed in ±(001) polar planes can grow on the surface of glass substrate.[37] Single crystalline slices sandwiched in predominant ±(001) polar surfaces can be generated on the surface of glass substrate by utilizing PEG additive in solution synthesis.[39] Organic dyes also inhibit the growth of ZnO nanocrystals along their ⟨0001⟩ and lead to the formation of ZnO films consisting of closely packed disks incased in ±(001) polar facets.[40] Recently, dense ⟨0001⟩ oriented polycrystalline ZnO films made by adding citrate into wet chemical reactions show excellent optical properties.[41] In particular, inorganic additives can result in the formation of thin films consisting of ZnO crystals terminated with (001) basal planes.[42] However, most of the ZnO supercrystals exposed in polar ±(001) facets have been grown on the surfaces of substrates, and the ZnO slices sandwiched

* Address correspondence to lifeng696@yahoo.com, fengli@zzuli.edu.cn.

Received for review February 13, 2013 and accepted November 19, 2013.

Published online November 19, 2013
10.1021/nn404591z

between their ±(001) polar planes generally stack closely to form mesocrystals for the dipole−dipole interactions attributed to the polar surfaces terminated with a Zn^{2+} plane and an O^{2-} plane, respectively.

In addition to 1D and 2D crystals, 0D nano/microspheres are also thought to be attractive materials for applications such as drug delivery, sensors, photonics, and solar cells.[42−48] Compared to ZnO nanocrystals in 1D and 2D, ZnO spheres are relatively rare in literature for their intrinsic nature of anisotropic growth, and they are usually composed of ZnO nanoparticles or nanoplatelets in smaller sizes.[46,49−54] For example, ZnO microspheres composed of mesocrystalline layers were synthesized by using poly(sodium 4-styrenesulfonate) to direct the growth of ZnO crystals.[53] The dipole−dipole interaction between the ±(001) polar surfaces also play a crucial role in the formation of the mesocrystalline ZnO spheres. The closely stacked ZnO mesostructures, however, could inevitably affect and possibly reduce their performances in applications related to the higher energy of ±(001) facets. In particular, the surface topography is one of the most important topics substantially influencing the properties of materials,[47,55] and the shape of nanocrystals is therefore a relevant area of focus in materials science for its diverse potentials in tailoring the functionalities of materials associated with surface energy of specific facets.[24,56−58] However, to the best of our knowledge, there is no report in literature concerned with the growth of 0D ZnO supercrystals topologically exposed in ±(001) facets and their optical functionalities depending on the special structures so far.

Driven by understanding and improving the functionalities of materials related to their microstructures, we have worked on constructing nanoarchitectures with well-controlled structures for identifying the linear answers to their properties.[59−65] Recently, we have successfully made 3D nanoarchitectures—porous Co_3O_4 twin-spheres with a sea urchin-like structure with an approach based on multistep splitting growth from 1D nanorods.[62] Hexagonal ZnO discs and rings terminated with ±(001) facets at their top and bottom surfaces, respectively, can be produced by adding sodium bis(2-ethylhexyl) sulfosuccinate (AOT) into an oil-in-water two-phase solution synthesis.[66] Herein we further harness the growth behaviors of 0D ZnO crystals for producing ZnO twin-spheres with topological surfaces exposed in ±(001) facets. The effects of surfactant and reaction time on the structures of ZnO supercrystals have been carefully investigated to understand the formation of the twin-spheres. A series of ZnO superstructures including prisms, dumbbells, twin-spheres exposed in ±(001) facets, and twin-spheres covered with dots have been produced in large scale by adjusting the molar ratio of AOT to Zn^{2+} ions ranging from 8:1 to 0.5:1. It was found that the growth of ZnO supercrystals starts from 1D prisms,

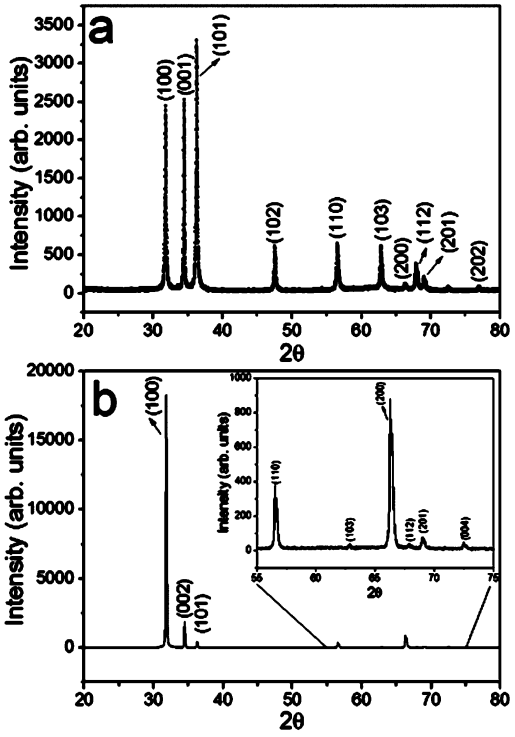

Figure 1. XRD profiles of ZnO (a) twin-spheres exposed in ±(001) facets and (b) prisms.

which act not only as seeds for growth, but also as bridges to connect the two hemispheres of twin-spheres. ZnO supercrystals exposed in ±(001) facets can be produced eventually, after growing for 8−12 generations and sealing a hollow ring inside each of particles. Based on the experimental results, a stepwise self-assembly mechanism is proposed to understand the formation of ZnO twin-spheres topologically exposed in ±(001) facets. In particular, it was also found that the ZnO twin-spheres show unique emission behaviors—anisotropic blue emission in intensity corresponding to their two hemispheres, which could be attributed to the polar surfaces of the two hemispheres terminated with Zn^{2+} planes and O^{2-} planes, respectively. The anisotropic emission of as-prepared ZnO supercrystals indicate that novel devices could be designed and fabricated through tailoring the microstructures of materials carefully.

RESULTS AND DISCUSSION

The ZnO twin-spheres were synthesized with a two-phase solution method involving (1) the preparation of oil-in-water micromicelles, $Zn(NO_3)_2$/water/1-butanol, with the help of AOT at molar ratio of AOT to Zn^{2+} at 2:1, and (2) the subsequent growth of ZnO supercrystals in the micromicelles at 90 °C. The as-prepared white powders were first characterized with X-ray diffraction (XRD) to verify their composition (Figure 1a). All of the diffraction peaks can be indexed as wurtzite (hexagonal) ZnO phase with lattice constants of $a = b = 0.3249$ nm, $c = 0.5205$ nm. The sharp reflection peaks of

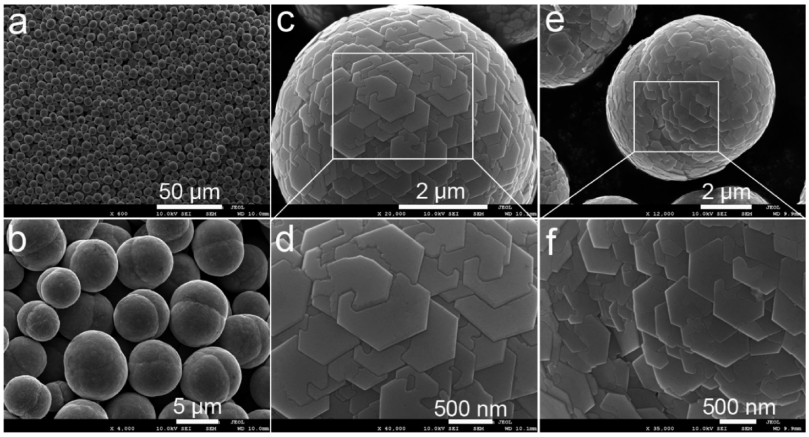

Figure 2. FESEM images of ZnO disc-twin-spheres with topological surfaces. (a, b) Low magnification images of the disc-twin-spheres; (c) top view of one disc-twin-sphere and (d) its high magnification image highlighted in the white box in c; (e) side view of one twin-sphere and (f) its high magnification image shown in the white box in e.

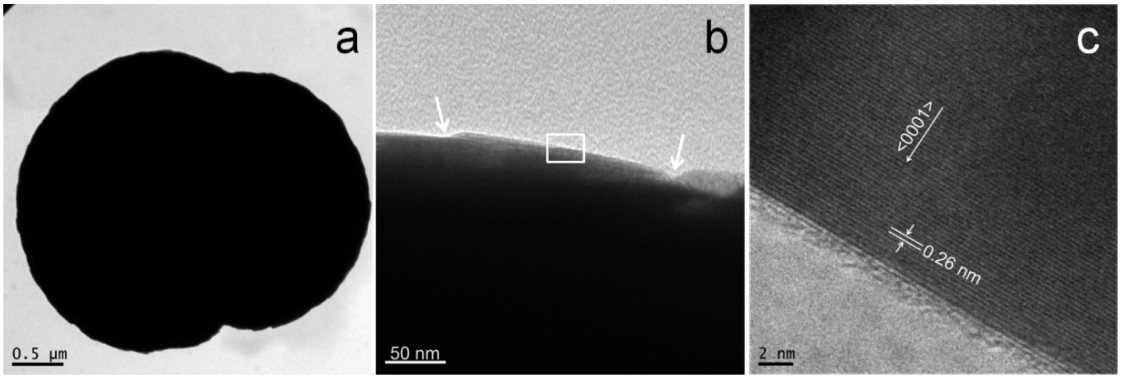

Figure 3. TEM images (a, b) of ZnO disc-twin-spheres and the HRTEM image (c) of the disc-twin-sphere highlighted with white box in b.

the XRD pattern suggest that the ZnO products (JCPDS Card No. 36-1451) are of highly crystalline. Compared to diffraction peaks attributed to (100) facet in standard diffraction pattern, the relative intensity of (001) plane is enhanced in the XRD profile. This indicates the higher concentration of (001) facets in the materials. In comparison, the XRD profile (Figure 1b) of ZnO prisms (field-emission scanning electron microscopy (FESEM) and transmission electron microscopy (TEM) images, see Figures S1−3) synthesized at 7:1 molar ratio of AOT to Zn^{2+} reveals that the relative intensity of the diffraction peak attributed to (100) plane is much higher than that of those aroused by (001) and (101) facets. There is no other diffraction peaks detected, which indicates that there is no impurity existing in the final product (5% deviation).

Figure 2a−b shows typical low magnification FESEM images of ZnO twin-spheres of *ca.* 5 and 8 μm in diameters along their short and long axis, respectively. The ZnO spheres produced by conducting the reaction at 2:1 molar ratio of AOT to Zn^{2+} ions are pure and uniform in size and are dominated by twin-spheres with well-defined shape. Each of the twin-spheres consists of two hemispheres with a concave groove to join them together at their waists. The top views of the twin-spheres (Figure 2c, Figure S4−5) reveal the puzzle-like patterns on their surfaces—topological surfaces covered with small facets of *ca.* 1 μm in diameter. Figure 2d further highlights the surface structure of the twin-sphere at higher magnification. The fragmentary and hexagonal facets all link with one another on the curved surface of the sphere. While the size and shape of the hexagonal facets vary dramatically, they connect and buckle together with bolts to form topological patterns. Figure 2e−f and Figure S6 show side view of the ZnO twin-spheres. The hexagonal facets orient along the curved surfaces of the twin-spheres gradually and merge at their waists. The small facets, which match exactly one another, self-assemble closely to form ZnO twin-spheres with topological surfaces. More microstructure details of the ZnO twin-spheres can be revealed by TEM observation as shown in Figure 3. While the dark and uniform contrast of the twin-spheres (Figure 3a) resulted from their big size implies that the spheres with topological surface could be solid, more evidence to be presented later indicate that there is a hollow ring buried inside each of the supercrystals. The higher magnification TEM image

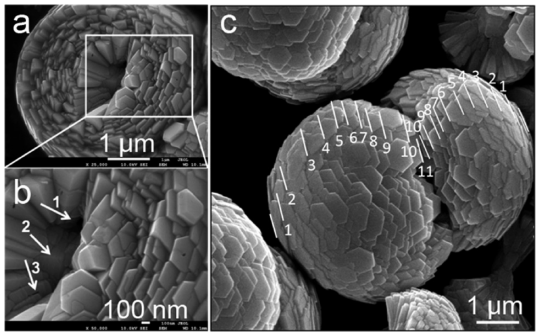

Figure 4. (a,b) Cross-section and (c) side view of ZnO twin-spheres produced at 4:1 molar ratio of AOT to Zn^{2+} ions.

taken at the edge of the sphere further shows that the sphere is covered with flat and smooth facets as shown in Figure 3b. Kinks and steps (highlighted with white arrows in Figure 3b), which closely adjoin the small facets on the curved surface of the twin-spheres, can be observed. Figure 3c shows high resolution TEM (HRTEM) image of the twin-sphere taken at the location highlighted with white box in Figure 3b. The lattice spacing of 0.26 nm corresponds to the *d*-spacing of (001) crystal planes of ZnO. The ZnO twin-spheres have been incased in ±(001) polar planes. The HRTEM images (Figure S7) taken around a twin-sphere at different locations further confirm that the hexagonal facets on the surfaces of ZnO twin-spheres are ±(001) planes. A thin and amorphous layer of *ca.* 1 nm in thickness, which could be aroused by the surface protection of surfactant molecule, can be observed on the surface of the spheres.

The cross-sectional image of one twin-sphere presented in Figure 4a−b can reveal the growth behaviors of the ZnO supercrystals exposed in ±(001) facets. It can be observed clearly that the supercrystals are composed of ZnO nanowedges closely attaching each other and arranging in radial symmetry. A hollow ring (arrow 1 in Figure 4b) around a prism (arrow 2 in Figure 4b), which bridges the two hemispheres together, has been sealed inside the twin-sphere. The side view of a ZnO twin-sphere (Figure 4c and Figures S8−9) shows a deep pit around the waist of the twin-sphere. The white lines on its surface highlight the growth generations on the surfaces of the two topological hemispheres consisting of the twin-sphere. The hexagonal facets tilt step-by-step to form hemispheres with topological surfaces. While the dimension and tilt angle of each generation of the facets vary, it is interesting to find out that the hemispheres can be generated after tilting for 8−11 generations. The equators of hemispheres can be approached, after the nanowedges self-assemble for *ca.* 5 generations. We can thus estimate that each step of the facets tilts for about 18° on average. Defects resulted from the stress on the tilted facets can be observed on the surface of the twin-spheres (Figure 2d and Figure S5).

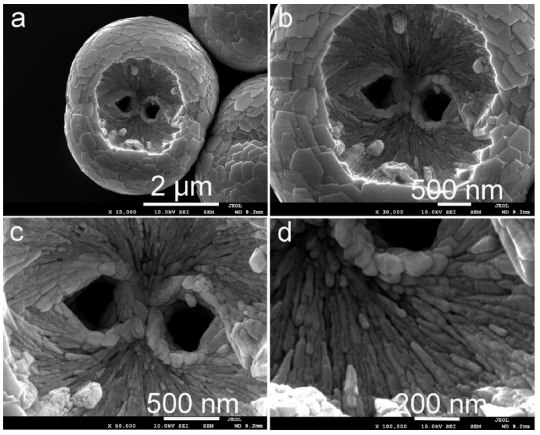

Figure 5. Interior structure of a supercrystal opened at its central area.

The stepwise self-assembly growth of the ZnO supercrystals can be verified clearly by one twin-sphere opened at its central area as shown in Figure 5. A crater of *ca.* 2 μm (Figure 5a−b) in diameter was dug out at the waist of the twin-sphere. It can be observed that there are two small pits of *ca.* 400 nm in diameter, which are separated by a prism of *ca.* 500 nm in diameter, in the crater. The results reveal undoubtedly that hollow twin-spheres are produced: A hollow ring has been sealed inside the twin-sphere around a prism. The SEM images at higher magnification (Figure 5c−d) of the crater show that ZnO nanowedges, which act as nanosized building blocks, go from the prism at the central area and self-assembly to form radial symmetry inside the supercrystals. The self-assembled interior structure of the supercrystals can be further revealed by their cross-sectional view as shown in Figure S10. The ZnO nanowedges meet at the waist of the supercrystals, and therefore a hollow ring is sealed inside each of them eventually.

In order to further understand the formation of the topological twin-spheres, the effects of AOT surfactant and reaction time on the microstructure of ZnO particles were investigated carefully. Figure 6 shows the surfactant effect on the microstructure of the ZnO particles, which clearly indicate that the formation of the ZnO twin-spheres is strongly dependent on the molar ratio of surfactant to Zn^{2+} ions. Conducting the reaction at 8:1 molar ratio of AOT to Zn^{2+} ions can only generate ZnO prisms (Figure 6a1−3) in the reaction. In accompanying with lowering the amount of surfactant in the reaction to 4:1, however, twin-spheres topologically incased in (001) facets (Figure 6b1−3 and Figure S11) can be produced on a large scale. However, deep pits can be observed at the waists of most twin-spheres produced at 4:1. In contrast, twin-spheres with concave grooves at their waists as shown in Figure 2 and Figure 6c1−3 can be synthesized, after conducting the reaction at a 2:1 molar ratio. The twin-spheres

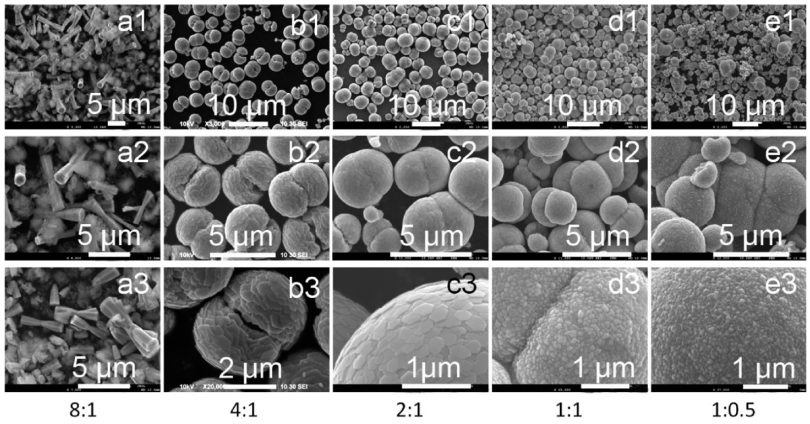

Figure 6. ZnO superstructures produced at molar ratio of AOT to Zn^{2+} from (a) 8:1 to (e) 1:0.5.

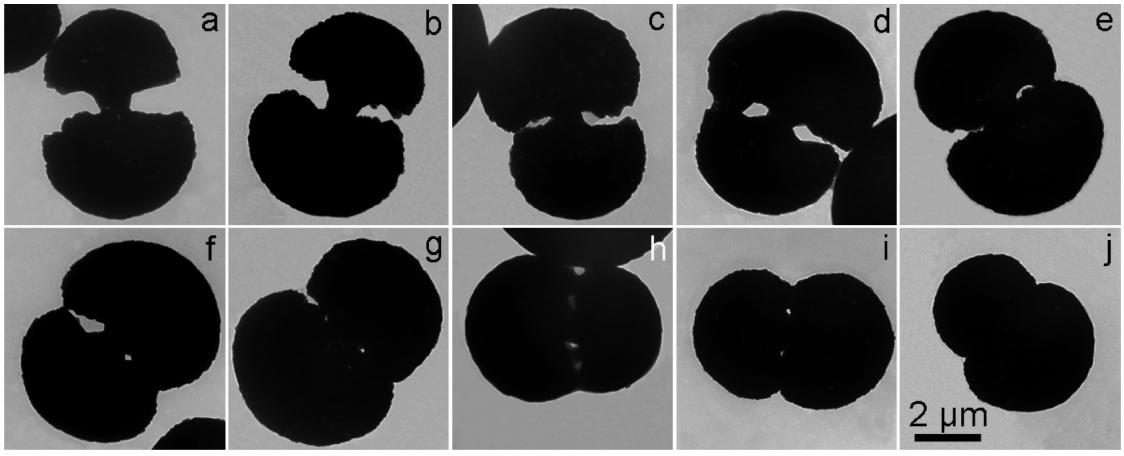

Figure 7. Structure evolution of ZnO twin-spheres prepared at different molar ratio of AOT to ZnO^{2+} ions. (a−c) Two hemispheres bridged with a prism produced at 5:1; (d−f) twin-spheres closed at one side produced at 4:1; and (g−i) a hollow ring formed around prism and (j) twin-spheres sealed at their waists finally produced at 2:1.

(Figure 6c1−3) fabricated at 2:1 show much smoother surfaces than those produced at a molar ratio of 4:1.

The experimental observations indicate that the growth rate of ZnO crystals can be inhibited dramatically, after adding more surfactant into the reaction system. It is interesting to find out that the surface structure of the twin-spheres further change from hexagonal facets into small irregular particles of about 40 nm in diameter to get twin-spheres covered with dots (Figure 6d1−3 and Figure S12), after further reducing the amount of surfactant used in the reaction to 1:1 molar ratio. When the reaction is conducted at a 0.5:1 molar ratio, only are ZnO particles with random size and shape (Figure 6e1−3) generated, because there is no efficient protection from the surfactant during crystal growth. Apparently, a suitable amount of AOT is critical to the formation of ZnO twin-spheres exposed in ±(001) facets, and the optimized molar ratio of AOT to Zn^{2+} ions is in the range of 2:1 to 4:1. The surfactant molecules, which can form micromicelles as nanoreactors to direct the formation of ZnO twin-spheres with defined size and shape, may prefer selectively binding onto the ±(001) facets of ZnO crystals.[66] A thin and amorphous layer of *ca.* 1 nm in thickness as shown in TEM image (Figure 3c), which corresponds to the length of AOT molecule, clearly shows the protection from the surfactant on the surface of ±(001) facets. ZnO twin-spheres exposed in ±(001) facets can be therefore produced in the reaction at a molar ratio ranging from 2:1 to 4:1. However, more surfactant added into the reaction can lead to the formation of ZnO prisms for dramatically reducing the growth rate. ZnO prisms (Figure S1−3), dumbbells (Figure S13−14), twin-spheres exposed in ±(001) facets (Figure 3, Figure S4−9 and Figure S11), and twin-spheres covered with dots (Figure 6d1−3 and Figure S12) can be produced on a large scale by carefully adjusting the amount of surfactant used in the synthesis. The dynamic growth of ZnO supercrystals can also be revealed by reaction time effect on their structure (Figure S15). TEM observation as shown in Figure 7 can further verify the structure evolution of ZnO supercrystals prepared at different molar ratios of AOT to ZnO^{2+} ions. The ZnO dumbbell grows gradually to form twin-spheres, and a ring around the prism can be sealed finally inside each of the twin-spheres.

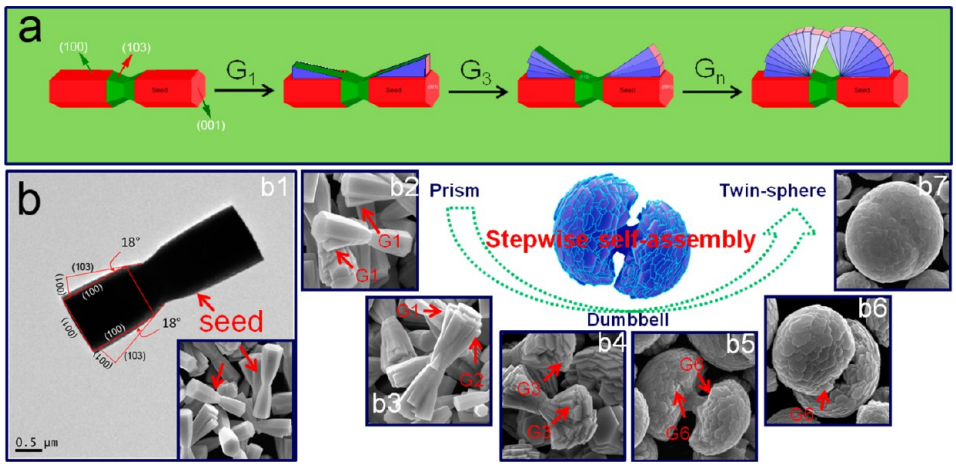

Figure 8. (a) Proposed stepwise self-assembly growth of ZnO twin-spheres topologically exposed in ±(001) facets. (b) TEM and SEM images of ZnO superstructures. (b1) TEM and SEM images of ZnO seed—prisms produced for the fast growth along ⟨0001⟩; (b2) the first and (b3) the second generation of self-assembly growth of prisms on the surface of ZnO seeds; (b4) ZnO dumbbells obtained by growing for more than three generations; (b5) ZnO dumbbell obtained by growing for about 6 generations; (b6) ZnO twin-sphere with a deep pit produced by growing for 8−12 generations; and (b7) ZnO twin-spheres with a concave groove at their waists.

Based on the experimental observation, a stepwise self-assembly mechanism as shown in Figure 8a is proposed to understand the formation of ZnO twin-spheres topologically exposed in ±(001) facets. Self-assembly is a strategy utilized to spontaneously construct complex or hierarchical objects with well-defined structures with building blocks such as inorganic ions/anions, organic molecules/polymers, and inorganic nanocrystals. Among the techniques developed based on self-assembly, the self-assembly growth of inorganic supercrystals, which employs inorganic ions/anions or nanocrystals as building blocks for building complex architectures, is similar to supermolecule self-assembly and cooperative self-assembly. (1) While the shapes of crystals are expected to reflect their unit-cell replication and amplification, their morphologies such as ZnO crystal's superstructures often vary significantly from the shape of their unit-cell due to the difference in surface energy of their facets. (2) Because the growth of ZnO supercrystals are confined in the micromicelles, nanoreactors constructed with AOT,[21] ZnO particles with uniform size can be produced on a large scale. The fast growth nature of ZnO crystals can lead to the formation of ZnO prisms as shown in Figure 8b1. (3) Based on the Wolff's rule,[67] then, the continued growth of ZnO crystals prefers to take place at the steps and kinks on their surfaces for the higher surface energy at the locations, compared to that of the flat plane. The first generation of the growth therefore starts at the central areas from the (103) facets of the seeded ZnO prisms (Figure 8b2 and Figures S1−3) for the higher density of defects and higher energy at the areas, in accompanying with adding less AOT into the reaction to enhance the growth rate. A wedge extended from (103) facet is therefore generated on the (100) facets of ZnO prisms (Figure 8aG1 and b2). More kinks and steps can be thus yielded on the surfaces of ZnO crystals, because of the first generation growth around the seeded prisms. The self-assembly growth starting from (103) facets in the central areas of the prisms can finally result the formation of nanowedges tilting 18° from the surfaces of the prisms (Figure 8b1). The results are also consistent with the structure analysis from SEM images in Figure 4c. (4) Subsequently, the second generation of the self-assembly growth (Figure 8b3) can occur at the kinks and steps for the higher energy at the locations. The ZnO nanowedges terminated with ±(001) facts at their bigger ends attaches closely and radially around the surfaces of ZnO prisms to form topological superstructure. (5) ZnO dumbbells (Figure 8b4 and Figures S13−14) can be produced, after growing for more than three generations. A stem (Figure 8b5), which connects two hemispheres to form a dumbbell, can be observed clearly, after growing for about 5 generations. (6) After growing for 8−12 generations (Figure 8b6), the ZnO nanowedges can eventually assemble into twin-spheres. (7) ZnO twin-spheres (Figure 8b7) can be produced on a large scale, after further growing to seal a hollow ring around a prism inside (Figure 4−5 and Figures S8−9). The hollow structure of ZnO twin-spheres can be observed clearly in TEM images as shown in Figure 7 also. Due to the two ends of ZnO prisms are covered by polarized ±(001) facets, respectively, which could result in rate difference of their growth, the sizes of the two hemispheres of ZnO twin-spheres generated from the seeds are different. The stepwise structure evolution of the twin-spheres supports the self-assembly mechanism proposed well. (8) The surfactant could play three roles critical in the formation of ZnO twin-spheres: The first, lowering the energy of ±(001) facets through binding

the planes selectively; the second, reducing the growth rate of ZnO crystals for the stepwise self-assembly growth; and the third, confining the growth of ZnO particles to produce uniform twin-spheres. The stepwise self-assembly growth of the ZnO supercrystals finally yield twin-spheres topologically encased in ±(001) facets, which are dictated by the surfactant used in the synthesis as shown in Figure S16.

The optical property and microstructures of ZnO twin-spheres can be further characterized with optical and luminescent microscopes as shown in Figure 9. The optical images show that there is a black shell on the surfaces of each sphere as shown in the left column of Figure 9. It is interesting to find out that there is a black ring locating at the central area of each sphere (Figure 9c and e), which could be resulted from the difference in the refractive indexes between ZnO crystal and air. The results further verify the special interior structure of the twin-spheres: A hollow ring around a prism has been sealed inside each of the twin-spheres. In addition, for all of the twin-spheres, the luminescence is strong enough to observe the emission of single twin-sphere in a conventional optical microscopy setup. The corresponding luminescent images of the twin-spheres are depleted in the right column of Figure 9. While the twin-spheres emit blue light as expected, it is a surprise to find that the supercrystals exhibit anisotropic emissions in intensity at their surfaces (Figure 9d and f). Recently, the first principle studies of ZnO crystals reveal that the dipolar ±(001) facets of ZnO can emit blue light at the same wavelength, but the intensity of the emission attributed to (001) facets terminated with O^{2-} is much stronger than that of (001) planes terminated with Zn^{2+} ions.[68] While the as-prepared twin-spheres consist two hemispheres with similar morphology, the two hemispheres could be terminated with O^{2-} and Zn^{2+} planes, respectively, and thus show anisotropic emission. In particular, much stronger emissions can be observed at the central areas of the twin-spheres. This could be attributed to the special surface structure of the twin-spheres also. It was reported that semiconductor nanocrystals can be used as waveguides.[2c] The ZnO nanowedges, which self-assemble radially to form the twin-spheres, can guide their emissions to the central areas of the twin-spheres and thus result in strong emissions there. In contrast, the optical and luminescent images (Figure S17−18) of ZnO prism and twin-spheres covered with dots indicate that they uniformly emit blue light only. The results further support that the blue emissions including anisotropic emission and strong emission at the central area of ZnO twin-spheres are attributed to their special superstructure: topological surfaces exposed in ±(001) facets and a hollow ring around prism inside each of the particles. The anisotropic emission also indicates that the ZnO twin-spheres exposed in ±(001) facets are a new class of Janus particles.

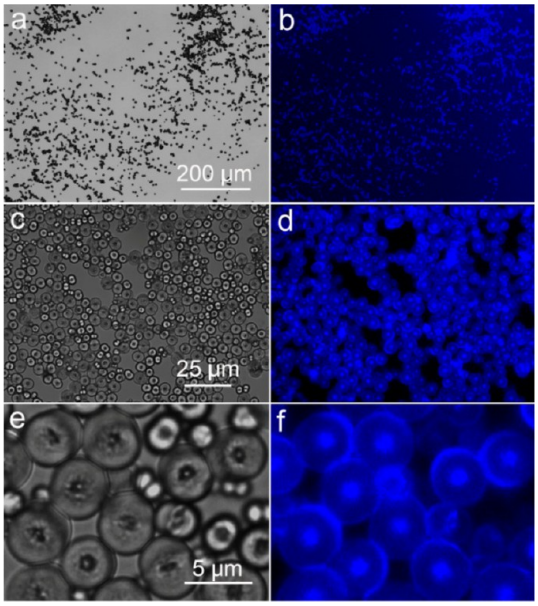

Figure 9. (a,c,e) Optical and (b,d,f) photoluminescence images of ZnO twin-spheres topologically exposed in (001) facets.

CONCLUSIONS

In summary, a series of ZnO supercrystals with well-controlled microstructures have been successfully synthesized on a large scale. The AOT surfactant, which is added into the reactions for establishing stable micromicelles as nanoreactors, can dramatically affect the structures of ZnO supercrystals. The morphology of ZnO supercrystals evolves from prism to dumbbell and to twin-sphere exposed in ±(001) facets eventually, in accompanying with adjusting the molar ratio of AOT to Zn^{2+} ions. The stepwise self-assembly mechanism, which is proposed to understand the formation of the ZnO twin-spheres, could be applied to construct nanoarchitectures with diverse materials and tailor their functionalities. The special blue emissions of ZnO twin-spheres exposed in ±(001) facets demonstrate that novel optical devices could be designed and fabricated by tailoring the surface topology of the materials.

METHODS

Synthesis of ZnO Twin-Spheres Exposed in ±(001) Planes. ZnO twin-spheres were synthesized with a two-phase solution method involving the preparation of oil-in-water micromicelles, $Zn(NO_3)_2$/water/1-butanol, with the help of sodium bis(2-ethylhexyl) sulfosuccinate (AOT) at a molar ratio of AOT to Zn^{2+} ion from 2:1 to 4:1. Typically, an AOT microemulsion was first prepared by adding an aqueous solution of $Zn(NO_3)_2 \cdot 6H_2O$

(0.025 mol in 90 mL of H_2O) to a solution of AOT (0.05 mol) in 1-butanol (10 mL) and vigorously stirring for 5 h. The volume ratio of the aqueous phase to the organic phase was 9:1. Then a concentrated aqueous solution of $NH_3 \cdot H_2O$ (17.65 M) with a 4:1 molar ratio to $Zn(NO_3)_2 \cdot 6H_2O$ was added dropwise to the well-stirred microemulsion. The solution was stirred for 5 h at room temperature, after adding concentrated aqueous solution of $NH_3 \cdot H_2O$. The milky white mixture produced was subsequently kept at 90 °C for 8 h to yield a white suspension. The precipitate was separated by centrifugation and washed for 5 times with distilled water and absolute ethanol, respectively. A white powder was produced finally by drying at 70 °C in vacuum for 24 h.

Synthesis of ZnO Prisms. ZnO prisms were synthesized with the method similar to the synthesis of ZnO twin-spheres. The reaction parameters were kept identical, except for the molar ratio of AOT to Zn^{2+} ions. ZnO prisms can be produced at a molar ratio ranging from 6:1 to 8:1.

Synthesis of ZnO Dumbbells. ZnO dumbbells were also synthesized with the method similar to the synthesis of ZnO twin-spheres. The reaction parameters were kept identical, except for the molar ratio of AOT to Zn^{2+} ions. ZnO dumbbells can be produced at a 5:1 molar ratio of AOT to Zn^{2+} ions.

Synthesis of ZnO Twin-Spheres Covered with Dots. ZnO twin-spheres covered with dots were synthesized with the method similar to the synthesis of ZnO twin-spheres also. The reaction parameters were kept identical, except for the molar ratio of AOT to Zn^{2+} ions at 1:1.

Characterization. The as-prepared products were characterized by powder XRD using a D/max 2550 V X-ray diffractometer (Rigaku, Tokyo, Japan) with monochromatized Cu Kα (λ = 1.54056 Å; scanning rate: 0.02 deg·s^{-1}) in the range of 10−90° incident radiation. The transmission light microscope and fluorescence microscope of the ZnO particles were collected with a Nikon Eclipse 80i microscope equipped with a Cool Snap HQ2 CCD camera. Room-temperature photoluminescence (PL) spectra were measured using a 0.5-m-long 9040 ScienceTech monochromator coupled with a Hamamatsu PMH-04 photomultiplier. The 325 nm emission of a He−Cd laser source (Melles Griot) of 10 mW power was used for exciting the samples. The morphologies and the structures of all of the products were analyzed by FESEM (JSM-7001F), TEM, HRTEM, and SAED (JEM-2100 operated at 200 kV). The cross-sectional images of ZnO twin-spheres were obtained by treating the particles with O_2/Ar plasma in a EQ-PDC-32G plasma cleaner. The particles dispersed in EtOH were deposited onto the surface of a piece of glass slide and dried in air and then placed into the chamber of plasma cleaner. The facets on the surface of the twin-spheres were destroyed, after being treated in O_2/Ar plasma for 5 min. The cross-section of the twin-sphere was produced by etching for 20 min.

Conflict of Interest: The authors declare no competing financial interest.

Acknowledgment. This work was supported by NSFC (NSFC. 21071130 and 21371157), Outstanding Scholar Program of Henan Province (114200510012) and Key Program of Henan Province in Science and Technology (132102210424, 92102310334, and 112102210239). The authors would like to give our thanks to Professor Z. L. Wang at School of Materials Science & Engineering, Georgia Institute of Technology for his constructive comments on the paper. The authors would like to dedicate the paper to Professor X. Xin at Nanjing University for the event of his 80th birthday.

Supporting Information Available: TEM images and SEM images of ZnO prisms, dumbbells, and twin-spheres exposed in ±(001) facets with different structures; cross-sectional images of twin-spheres; transmission optical images and photoluminescence images of ZnO prisms and twin-spheres covered with dots; photoluminescent spectra of ZnO prisms, dumbbells and twin-spheres. This material is available free of charge *via* the Internet at http://pubs.acs.org.

REFERENCES AND NOTES

1. Xu, S.; Qin, Y.; Yu, C.; Wei, Y.; Yang, R.; Wang, Z. L. Self-Powered Nanowire Devices. *Nat. Nanotechnol.* **2010**, *5*, 366–373.
2. Wang, Z. L.; Song, J. Piezoelectric Nanogenerators Based on Zinc Oxide Nanowire Arrays. *Science* **2006**, *312*, 242–246.
3. Pan, Z. W.; Dai, Z. R.; Wang, Z. L. Nanobelts of Semiconducting Oxides. *Science* **2001**, *291*, 1947–1949.
4. Gao, P. X.; Wang, Z. L. Mesoporous Polyhedral Cages and Shells Formed by Textured Self-Assembly of ZnO Nanocrystals. *J. Am. Chem. Soc.* **2003**, *125*, 11299–11305.
5. Xu, C.; Wang, X.; Wang, Z. L. Nanowire Structured Hybrid Cell for Concurrently Scavenging Solar and Mechanical Energies. *J. Am. Chem. Soc.* **2009**, *131*, 5866–5872.
6. Wei, T.-Y.; Yeh, P.-H.; Lu, S.-Y.; Wang, Z. L. Gigantic Enhancement in Sensitivity Using Schottky Contacted Nanowire Nanosensor. *J. Am. Chem. Soc.* **2009**, *131*, 17690–17695.
7. Kong, X. Y.; Wang, Z. L. Spontaneous Polarization-Induced Nanohelixes, Nanosprings, and Nanorings of Piezoelectric Nanobelts. *Nano Lett.* **2003**, *3*, 1625–1631.
8. Wang, X.; Summers, C. J. S.; Wang, Z. L. Large-Scale Hexagonal-Patterned Growth of Aligned ZnO Nanorods for Nano-Optoelectronics and Nanosensor Arrays. *Nano Lett.* **2004**, *4*, 423–426.
9. Yang, R.; Ding, Y.; Wang, Z. L. Deformation-Free Single-Crystal Nanohelixes of Polar Nanowires. *Nano Lett.* **2004**, *4*, 1309–1312.
10. Gao, P. X.; Ding, Y.; Mai, W. J.; Hughes, W. L.; Lao, C. S.; Wang, Z. L. Conversion of Zinc Oxide Nanobelts into Superlattice-Structured Nanohelices. *Science* **2005**, *309*, 1700–1704.
11. Gao, P.; Mai, W.; Wang, Z. L. Superelasticity and Nanofracture Mechanics of ZnO Nanohelices. *Nano Lett.* **2006**, *6*, 2536–2543.
12. Kong, X. Y.; Ding, Y.; Yang, R.; Wang, Z. L. Single-Crystal Nanorings Formed by Epitaxial Self-Coiling of Polar Nanobelts. *Science* **2004**, *303*, 1348–1351.
13. Wang, X.; Song, J.; Liu, J.; Wang, Z. L. Direct-Current Nanogenerator Driven by Ultrasonic Waves. *Science* **2007**, *316*, 102–105.
14. Huang, M. H.; Mao, S.; Feick, H.; Yan, H.; Wu, Y.; Kind, H.; Weber, E.; Russo, R.; Yang, P. Room-Temperature Ultraviolet Nanowire Nanolasers. *Science* **2001**, *292*, 1897–1899.
15. Zhu, H.; Shan, C. X.; Yao, B.; Li, B.-H.; Zhang, J.-Y.; Zhang, Z.-Z.; Zhao, D. X.; Shen, D. Z.; Fan, X. W.; Lu, Y. M.; et al. Ultralow-Threshold Laser Realized in Zinc Oxide. *Adv. Mater.* **2009**, *21*, 1613–1617.
16. Lao, M.; Sirbuly, D. J.; Johson, J. C.; Goldberger, J.; Saykally, R. J.; Yang, P. Nanoribbon Waveguides for Subwavelength Photonics Integration. *Science* **2004**, *305*, 1269–1273.
17. Cole, J. J.; Wang, X.; Knuesel, R. J.; Jacobs, H. O. Integration of ZnO Microcrystals with Tailored Dimensions Forming Light Emitting Diodes and UV Photovoltaic Cells. *Nano Lett.* **2008**, *8*, 1477–1481.
18. Manekkathodi, A.; Lu, M. Y. C.; Wang, W.; Chen, L.-J. Direct Growth of Aligned Zinc Oxide Nanorods on Paper Substrates for Low-Cost Flexible Electronics. *Adv. Mater.* **2010**, *22*, 4059–4063.
19. Son, D. I.; Kwin, B. W.; Park, D. H.; Seo, W.-S.; Yi, Y.; Angadi, B.; Lee, C.-L.; Choi, W. K. Emissive ZnO-Graphene Quantum Dots for White-Light-Emitting Diodes. *Nat. Nanotechnol.* **2012**, *7*, 465–471.
20. Sun, B.; Sirringhaus, H. Surface Tension and Fluid Flow Driven Self-Assembly of Ordered ZnO Nanorod Films for High-Performance Field Effect Transistors. *J. Am. Chem. Soc.* **2006**, *128*, 16231–16237.
21. Liao, F.; Huang, Y.; Ge, J.; Zheng, W.; Tedsree, K.; Collier, P.; Hong, X.; Tsang, S. C. Morphology-Dependent Interactions of ZnO with Cu Nanoparticles at the Materials' Interface in Selective Hydrogenation of CO_2 to CH_3OH. *Angew. Chem., Int. Ed.* **2011**, *50*, 2162–2165.
22. Mclaren, A.; Valdes-Solis, T.; Li, G.; Tsang, S. C. Shape and Size Effects of ZnO Nanocrystals on Photocatalytic Activity. *J. Am. Chem. Soc.* **2009**, *131*, 12540–12541.

23. Jang, E. S.; Won, J.-H.; Hwang, S.-J.; Choy, J.-H. Fine Tuning of the Face Orientation of ZnO Crystals to Optimize Their Photocatalytic Activity. *Adv. Mater.* **2006**, *18*, 3309–3312.
24. Zhang, Y.; Xiang, Q.; Xu, J.; Xu, P.; Pan, Q.; Li, F. Self-Assemblies of Pd Nanoparticles on the Surfaces of Single Crystal ZnO Nanowires for Chemical Sensors with Enhanced Performances. *J. Mater. Chem.* **2009**, *19*, 4701–4706.
25. Hu, Y.; Zhou, J.; Yeh, P.-H.; Li, Z.; Wei, T. Y.; Wang, Z. L. Supersensitive, Fast-Response Nanowire Sensors by Using Schottky Contacts. *Adv. Mater.* **2010**, *22*, 3327–3332.
26. Guo, L.; Ji, Y. L.; Xu, H. Regularly Shaped, Single-Crystalline ZnO Nanorods with Wurtzite Structure. *J. Am. Chem. Soc.* **2002**, *124*, 14864–14865.
27. Liu, B.; Zeng, H. C. Hydrothermal Synthesis of ZnO Nanorods in the Diameter Regime of 50 nm. *J. Am. Chem. Soc.* **2003**, *125*, 4430–4431.
28. Greene, L. E.; Law, M.; Goldberger, J.; Kim, F.; Johnson, J. C.; Zhang, Y.; Saykally, R. J.; Yang, P. Low-Temperature Wafer-Scale Production of ZnO Nanowire Arrays. *Angew. Chem., Int. Ed.* **2003**, *42*, 3031–3034.
29. Yu, H.; Zhang, Z.; Han, M.; Hao, X.; Zhu, F. A General Low-Temperature Route for Large-Scale Fabrication of Highly Oriented ZnO Nanorod/Nanotube Arrays. *J. Am. Chem. Soc.* **2005**, *127*, 2378–2379.
30. Mo, M.-S.; Lim, S. H.; Mai, Y.-W.; Zheng, R.-K.; Ringer, S. P. *In Situ* Self-Assembly of Thin ZnO Nanoplatelets into Hierarchical Mesocrystal Microtubules with Surface Grafting of Nanorods: A General Strategy Towards Hollow Mesocrystal Structures. *Adv. Mater.* **2008**, *20*, 339–342.
31. Vayssieres, L. Growth of Arrayed Nanorods and Nanowires of ZnO from Aqueous Solutions. *Adv. Mater.* **2003**, *15*, 464–466.
32. Lao, J. Y.; Wen, J. G.; Ren, Z. F. Hierarchical ZnO Nanostructures. *Nano Lett.* **2002**, *2*, 1287.
33. Zhang, T.; Dong, W.; Keeter-Brewer, M.; Konar, S.; Njabon, R. N.; Tian, Z. R. Site-Specific Nucleation and Growth Kinetics in Hierarchical Nanosyntheses of Branched ZnO Crystallites. *J. Am. Chem. Soc.* **2006**, *128*, 10960–10968.
34. Sounart, T. L.; Liu, J.; Voigt, J. A.; Hsu, J. W. P.; Spoerke, E. D.; Tian, Z. R.; Jiang, Y. Sequential Nucleation and Growth of Complex Nanostructured Films. *Adv. Funct. Mater.* **2006**, *16*, 335–344.
35. Sounart, T. L.; Liu, J.; Voigt, J. A.; Huo, M.; Spoerke, E. D.; Mckenzie, B. Secondary Nucleation and Growth of ZnO. *J. Am. Chem. Soc.* **2007**, *129*, 15786–15793.
36. Tian, Z. R.; Voigt, J. A.; Liu, J.; Mckenzie, B.; Mcdermott, M. J.; Rodriquez, M. A.; Konishi, H.; Xu, H. Complex and Oriented ZnO Nanostructures. *Nat. Mater.* **2003**, *2*, 821–826.
37. Tian, Z. R.; Voigt, J. A.; Liu, J.; Mckenzie, B.; Mcdermott, M. J. Biomimetic Arrays of Oriented Helical ZnO Nanorods and Columns. *J. Am. Chem. Soc.* **2002**, *124*, 12954–12955.
38. Hsu, J. W. P.; Tian, Z. R.; Simmons, N. C.; Matzke, C. M.; Voigt, J. A.; Liu, J. Directed Spatial Organization of Zinc Oxide Nanorods. *Nano Lett.* **2005**, *5*, 83–86.
39. Liu, X.; Afzaal, M.; Ramasany, K.; O'Brein, P.; Akhtar, J. Synthesis of ZnO Hexagonal Single-Crystal Slices with Predominant (0001) and (0001) Facets by Poly(ethylene glycol)-Assisted Chemical Bath Deposition. *J. Am. Chem. Soc.* **2009**, *131*, 15106–15107.
40. Yoshida, T.; Minoura, H. Electrochemical Self-Assembly of Dye-Modified Zinc Oxide Thin Films. *Adv. Mater.* **2000**, *12*, 1219–1222.
41. Podlogar, M.; Richardson, J. J.; Vengust, D.; Daneu, N.; Samardžija, Z.; Bernik, S.; Rečnik, A. Growth of Transparent and Conductive Polycrystalline (0001)-ZnO Films on Glass Substrates Under Low-Temperature Hydrothermal Conditions. *Adv. Funct. Mater.* **2012**, *22*, 3136–3145.
42. Joo, J.; Chow, B. Y.; Prakash, M.; Boyden, E. S.; Jacobson, J. M. Face-Selective Electrostatic Control of Hydrothermal Zinc Oxide Nanowire Synthesis. *Nat. Mater.* **2011**, *10*, 596–601.
43. Lee, J. E.; Lee, N.; Kim, H. J.; Choi, S. H.; Kim, J. H.; Kim, T.; Song, I. C.; Park, S. P.; Moon, W. K.; Hyeon, T. Uniform Mesoporous Dye-Doped Silica Nanoparticles Decorated with Multiple Magnetite Nanocrystals for Simultaneous Enhanced Magnetic Resonance Imaging, Fluorescence Imaging, and Drug Delivery. *J. Am. Chem. Soc.* **2010**, *132*, 552–557.
44. Li, C. C.; Yin, X. M.; Wang, T. H.; Zeng, H. C. Morphogenesis of Highly Uniform $CoCO_3$ Submicrometer Crystals and Their Conversion to Mesoporous Co_3O_4 for Gas-Sensing Applications. *Chem. Mater.* **2009**, *21*, 4984–4992.
45. Wang, Y.; Ibisate, M.; Li, Z. Y.; Xia, Y. Metallodielectric Photonic Crystals Assembled from Monodisperse Spherical Colloids of Bismuth and Lead. *Adv. Mater.* **2006**, *18*, 471–476.
46. Zhang, Q.; Dandeneau, C. S.; Candelaria, S.; Liu, D.; Garcia, B. B.; Zhou, X.; Heong, Y.-H.; Cao, G. Effects of Lithium Ions on Dye-Sensitized ZnO Aggregate Solar Cells. *Chem. Mater.* **2010**, *22*, 2427–2433.
47. Kaufman, J. J.; Tao, G.; Shabahang, S.; Banaei, E.-H.; Deng, D. S.; Liang, X.; Johson, S. G.; Flink, Y.; Abouraddy, A. F. Structured Spheres Generated by an In-Fibre Fluid Instability. *Nature* **2012**, *487*, 463–467.
48. Yang, Y.; Liu, X.; Li, X.; Zhao, J.; Bai, S.; Liu, J.; Yang, Q. A Yolk–Shell Nanoreactor with a Basic Core and an Acidic Shell for Cascade Reactions. *Angew. Chem., Int. Ed.* **2012**, *51*, 9164–9168.
49. Agrawal, M.; Gupta, S.; Pich, A.; Zafeiropoulos, N. E.; Stamm, M. A Facile Approach to Fabrication of ZnO–TiO_2 Hollow Spheres. *Chem. Mater.* **2009**, *21*, 5343–5348.
50. Hu, X.; Gong, J.; Zhang, L.; Yu, J. C. Continuous Size Tuning of Monodisperse ZnO Colloidal Nanocrystal Clusters by a Microwave-Polyol Process and Their Application for Humidity Sensing. *Adv. Mater.* **2008**, *20*, 4845–4850.
51. Liu, B.; Zeng, H. C. Fabrication of ZnO "Dandelions" *via* a Modified Kirkendall Process. *J. Am. Chem. Soc.* **2004**, *126*, 16744–16746.
52. Wang, X.; Liao, M.; Zhong, Y.; Zheng, J. Y.; Tian, W.; Zhai, T.; Zhi, C.; Ma, Y.; Yao, J.; Bando, Y.; et al. ZnO Hollow Spheres with Double-Yolk Egg Structure for High-performance Photocatalysts and Photodetectors. *Adv. Mater.* **2012**, *24*, 3421–3425.
53. Liu, Z.; Wen, X. D.; Wu, X. L.; Gao, Y. J.; Chen, H. T.; Zhu, J.; Chu, P. K. Intrinsic Dipole-Field-Driven Mesoscale Crystallization of Core–Shell ZnO Mesocrystal Microspheres. *J. Am. Chem. Soc.* **2009**, *131*, 9405–9412.
54. Gu, Z.; Paranthaman, M. P.; Xu, J.; Pan, Z. W. Aligned ZnO Nanorod Arrays Grown Directly on Zinc Foils and Zinc Spheres by a Low-Temperature Oxidization Method. *ACS Nano* **2009**, *3*, 273–278.
55. Assender, H.; Bliznyuk, V.; Porfyrakis, K. How Surface Topography Relates to Materials' Properties. *Science* **2002**, *297*, 973–976.
56. Xiao, Y.; Lu, L.; Zhang, A.; Zhang, Y.; Sun, L.; Huo, L.; Li, F. Highly Enhanced Acetone Sensing Performances of Porous and Single Crystalline ZnO Nanosheets: High Percentage of Exposed (100) Facets Working Together with Surface Modification with Pd Nanoparticles. *ACS Appl. Mater. Interfaces* **2012**, *4*, 3797–3804.
57. Wang, H.; Koshizaki, N.; Li, L.; Jia, L.; Kawaguchi, K.; Li, X.; Pyatenko, A.; Swiatkowska-Warkocka, Z.; Bando, Y.; Golberg, D. Size-Tailored ZnO Submicrometer Spheres: Bottom-Up Construction, Size-Related Optical Extinction, and Selective Aniline Trapping. *Adv. Mater.* **2011**, *23*, 1865–1870.
58. Jang, E. S.; Won, J.-H.; Hwang, S.-J.; Choy, J.-H. Fine Tuning of the Face Orientation of ZnO Crystals to Optimize Their Photocatalytic Activity. *Adv. Mater.* **2006**, *18*, 3309–3312.
59. Li, F.; Zhu, M.; Liu, C.; Zhou, W. L.; Wiley, J. B. Patterned Metal Nanowire Arrays from Photolithographically-Modified Templates. *J. Am. Chem. Soc.* **2006**, *128*, 13342–13343.
60. Li, F.; Badel, X.; Linnros, J.; Wiley, J. B. Fabrication of Colloidal Crystals with Tubular-Like Packings. *J. Am. Chem. Soc.* **2005**, *127*, 3268–3269.
61. Li, F.; He, J.; Zhou, W. L.; Wiley, J. B. Synthesis of Porous Wires from Directed Assemblies of Nanospheres. *J. Am. Chem. Soc.* **2003**, *125*, 16166–16167.

62. Xiao, Y.; Liu, S.; Li, F.; Zhang, A.; Zhao, J.; Fang, S.; Jia, D. 3D Hierarchical Co_3O_4 Twin-Spheres with an Urchin-Like Structure: Large-Scale Synthesis, Multistep-Splitting Growth, and Electrochemical Pseudocapacitors. *Adv. Funct. Mater.* **2012**, *22*, 4052–4059.
63. Xiao, Y.; Zhang, A.; Liu, S.; Zhao, J.; Fang, S.; Jia, D.; Li, F. Free-Standing and Porous Hierarchical Nanoarchitectures Constructed with Cobalt Cobaltite Nanowalls for Supercapacitors with High Specific Capacitances. *J. Power Sources* **2012**, *219*, 140–146.
64. Xiao, Y.; Liu, S.; Fang, S.; Jia, D.; Su, H.; Zhou, W.; Wiley, J. B.; Li, F. Plum-Like and Octahedral Co_3O_4 Single Crystals on and Around Carbon Nanotubes: Large Scale Synthesis and Formation Mechanism. *RSC Adv.* **2012**, *2*, 3496–3501.
65. Xiao, Y.; Cao, Y.; Gong, Y.; Zhang, A.; Zhao, J.; Fang, S.; Jia, D.; Li, F. Electrolyte and Composition Effects on the Performances of Asymmetric Supercapacitor Constructed with Mn_3O_4 Nanoparticles-Graphene Nanocomposites, *J. Power Sources*, DOI: 10.1016/j.jpowsour.2013.07.118.
66. Li, F.; Ding, Y.; Gao, P.; Xin, X.; Wang, Z. L. Single-Crystal Hexagonal Disks and Rings of ZnO: Low-Temperature, Large-Scale Synthesis and Growth Mechanism. *Angew. Chem., Int. Ed.* **2004**, *43*, 5238–5242.
67. Meldrum, F. C.; Cölfen, H. Controlling Mineral Morphologies and Structures in Biological and Synthetic Systems. *Chem. Rev.* **2008**, *108*, 4332–4432.
68. Yamamoto, A.; Moriwaki, Y.; Hattori, K.; Yanagi, H. A Comparative Study of Photoluminescence of Zn-Polar and O-Polar Faces in Single Crystal ZnO Using Moment Analysis. *Appl. Phys. Lett.* **2011**, *98*, 061907.